EXPERIMENTAL INVESTIGATION OF THE ENERGY SEPARATION IN VORTEX TUBES

By H. H. Bruun*

Measurements of the state and the velocity distribution of air in a counterflow vortex tube have been undertaken. In order to determine the axial variation of the flow quantities, measurements were carried out in several cross-sections.

The experimental results show that the velocity is predominantly tangential. A comparison of the order of magnitude of the radial and axial convection terms in the equations of motion and energy shows that these terms are of equal importance.

The energy equation in terms of the total temperature $\bar{T}_0$ is used as a basis for discussing the influence of turbulence in the flow on the separation of energy in the vortex tube.

INTRODUCTION

SINCE Ranque (1)† discovered the ability of vortex tubes to separate compressed air into hot and cold air streams, experiments have been carried out with different types of vortex tubes. Most of these investigations have been undertaken with the counterflow and uniflow types, which are shown in Fig. 1*a* and *b* respectively.

The counterflow vortex tube (Fig. 1*a*) consists of an entrance block with a central orifice, a vortex tube and a valve. Compressed air enters the vortex tube tangentially through one or several nozzles. The mass flow of the inlet air is denoted as m_e, and the state of the air can be described by the static pressure P_e and the temperature T_e. In the vortex tube the air separates into a cold mass flow m_c and a hot mass flow m_h, which have the temperatures T_c and T_h respectively. The cold air is discharged into the atmosphere through the 'cold end' orifice, while the hot air flows out of the other end—the so called 'hot outlet'—along the periphery.

The geometry of the vortex tube can be described by the diameter of the vortex tube D, the diameter of the orifice d_c, the length of the vortex tube L, the geometry and number of nozzles and the design of the valve. The setting of the valve determines the ratio of the hot and cold mass flows, and is usually characterized by the mass ratio $\xi = m_c/m_e$.

The uniflow vortex tube (Fig. 1*b*) consists of an entrance block, a vortex tube and a valve with a central orifice. As the operation of the uniflow type is similar to the operation of the counterflow type, the same notation for the geometry and the flow quantities can be used.

The results of previous experimental investigations show that a considerable energy separation can occur in vortex tubes with widely different geometry. If P_e and T_e are kept constant, and the setting of the valve (and thereby ξ) is changed, a variation of the temperatures of the hot and cold mass flows T_h and T_c similar to the variation shown in Fig. 2 will occur.

The temperature drop of the cold mass flow $\Delta T_c = T_e - T_c$ is usually used to give a quantitative description of the energy separation. If the geometry and the setting of the valve are varied, experiments have shown that there exists a maximum value of the temperature drop ΔT_c for constant values of P_e and T_e. The corresponding geometry is usually referred to as the optimum geometry.

Early interest shown in the energy separation of the vortex tube was mainly due to the possible utilization of the vortex tube as a cooling device. As a result, the first investigations were mainly concerned with the determination of large temperature drops (ΔT_c) by variation of the geometry, the mass ratio ξ and the inlet pressure P_e. From these investigations very little could be deduced about the mechanism of the energy separation. Therefore experimental investigations of the state and velocity distribution of the gas in the vortex tube were initiated about 1950. Even so, a satisfactory explanation of the mechanism of the energy separation, which is in accordance with the flow inside the vortex tube, has not yet been published. The axial variation of the flow quantities has especially been neglected. As shown later this is rather a serious limitation.

An experimental set-up was therefore designed for measuring the velocity distribution and the state of

The MS. of this paper was received at the Institution on 10th July 1968 and accepted for publication on 19th May 1969. 33

* *Institute of Sound and Vibration Research, The University, Southampton.*

† *References are given in the Appendix.*

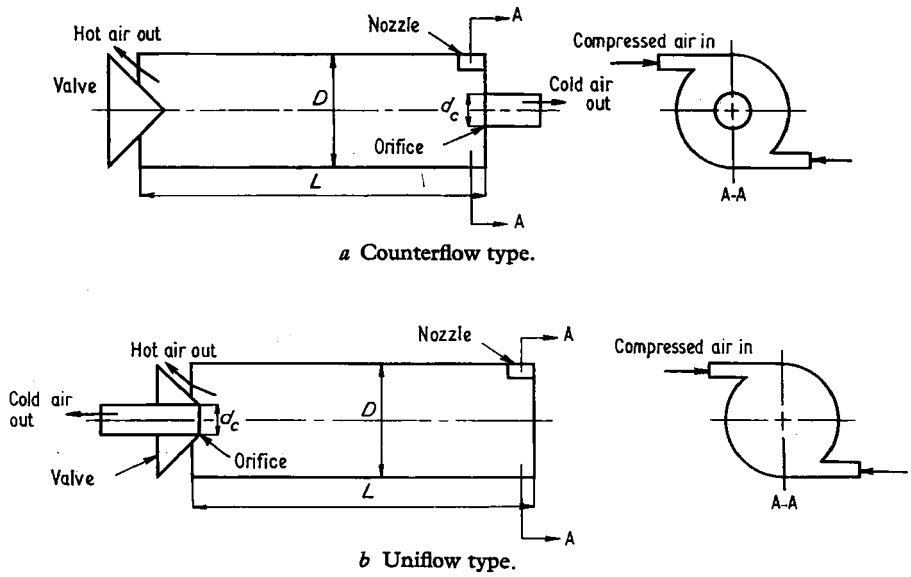

a Counterflow type.

b Uniflow type.

Fig. 1. *Schematic drawings of vortex tubes*

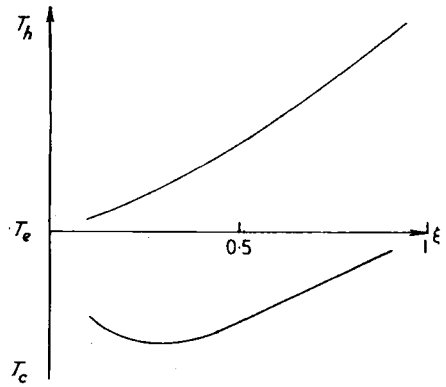

Fig. 2. *Temperature of hot and cold mass flows as functions of the mass ratio* ξ

the air in several cross-sections in a counterflow vortex tube.

Notation

c_p	Specific heat.
D	Diameter of vortex tube, $2R$.
d_c	Diameter of cold orifice.
d_e	Equivalent diameter of inlet nozzles, $\sqrt{\frac{4\times\text{inlet area}}{\pi}}$.
L	Length of vortex tube.
m_e, m_c, m_h	Mass flow of inlet air, cold air and hot air.
R_c	Radius of cold outlet pipe.
P, T, ρ	Static pressure, temperature and density.
r, θ, z	Radial, tangential and axial co-ordinates.
u, v, w	Radial, tangential and axial velocity components.
$\bar{u}, \bar{v}, \bar{w}$	Time mean value of radial, tangential and axial velocity components.
P_e, P_b	Static pressure of inlet air, barometric pressure.
$\bar{P}, \bar{P}_0, \bar{T}_0$	Time mean values of static pressure, total pressure and total temperature.
$\bar{P}_i, \bar{P}_{0i}, \bar{T}_{0i}, \bar{\alpha}_i$	Indicated time mean values of static pressure, total pressure, total temperature and flow angle.
T_e, T_c, T_h	Time mean values of total temperature of inlet air, cold air and hot air.
T_{ci}	Indicated temperature of cold air.
ΔT_c	$T_e - T_c$.
ΔT_{ci}	$T_e - T_{ci}$.
$\bar{T}_{ad}$	Adiabatic temperature distribution.
$\bar{T}_P$	Time mean values of temperature indicated by temperature probe.
$\bar{u}_{ab}$	Axial mean value of radial velocity between cross-sections *a* and *b*.
$\bar{\alpha}$	Time mean value of flow angle.
γ	c_p/c_v.
λ	Thermal conductivity.
μ	Dynamic viscosity.
ξ	m_c/m_e.

Subscripts

c	Cold.
e	Entry.
h	Hot.
i	Indicated.
0	Total.
t	Turbulent.

EXPERIMENTAL PROGRAMME

Experimental set-up

A vortex tube having a geometry close to the optimum geometry was designed based on previous investigations, and the author's own preliminary experiments. The vortex tube, which was made of Plexiglas, had a diameter $D = 94$ mm and a length $L = 520$ mm. The diameter of the cold orifice (d_c) and the equivalent diameter of the nozzles (d_e), as a result of the preliminary experiments, were given the values $d_c = 35$ mm and $d_e = 21{\cdot}5$ mm.

A schematic drawing of the experimental set-up is shown in Fig. 3. Compressed air flows into the entrance block through two 25 mm borings. From the ring chamber the air enters the vortex tube through four nozzles. The cold air is discharged through the cold end orifice into the atmosphere, while the hot air flows out of the other end of the vortex tube, which is closed by a diaphragm with discharge holes along the periphery, while the regulating valve has been moved to the end of the hot outlet pipe.

To diminish the noise from the outlets the ends of the hot and cold outlet pipes were placed in silencers as shown in the figure.

Along the length of the vortex tube and the cold outlet pipe ($R_c = 34{\cdot}5$ mm), ports 3 mm in diameter were placed for insertion of probes. The ports on the vortex tube were denoted by the numbers 0 to 10 and the ports on the cold outlet pipe by the numbers -1 to -3. The location of the ports is given in Fig. 3.

Instrumentation

The flow rates of the inlet air m_e and the hot air m_h were measured by the venturi tubes 1 and 3 in Fig. 3 respectively. From these measurements the cold mass flow m_c can be calculated as $m_c = m_e - m_h$. The inlet pressure P_e was measured by the mercury manometer 2.

The temperatures of the mass flows were measured with Chromel and Alumel thermocouples. The thermocouple 4 (Fig. 3) placed in the inlet pipe close to the entrance block measured the inlet temperature T_e. The temperature of the hot air T_h was measured by the thermocouple 5 placed in one of the discharge holes in the diaphragm at the hot end, and the temperature T_{c1}, measured by the thermocouple 6 placed in the centre of the cold outlet pipe, was used to indicate the temperature of the cold mass flow T_c. This temperature can be calculated from the temperature distribution in the cold outlet pipe.

Measurements inside the vortex tube were carried out with pressure and temperature probes. The measurements of the time mean values of the static pressure $\bar{P}$, the total pressure $\bar{P}_0$ and the flow angle $\bar{\alpha}$ were undertaken with 3 mm pressure probes of the type shown in Fig. 4*a*. To avoid 'end effects' on the measurements the three pressure taps were placed three diameters away from the tip. The angle between pressure taps 1 and 2 and between 2 and 3 was 60°, and the diameter of the pressure taps was 0·3 mm.

Two types of temperature probes (Fig. 4*b* and *c*) were used to determine the total temperature distribution in the vortex tube.

To reduce the heat conduction from the thermocouple junction to the support the Chromel and Alumel thermocouple wires were 0·2 mm diameter and the free length of the wires was 30 times the diameter. To obtain accurate measurements the pressure and temperature probes were

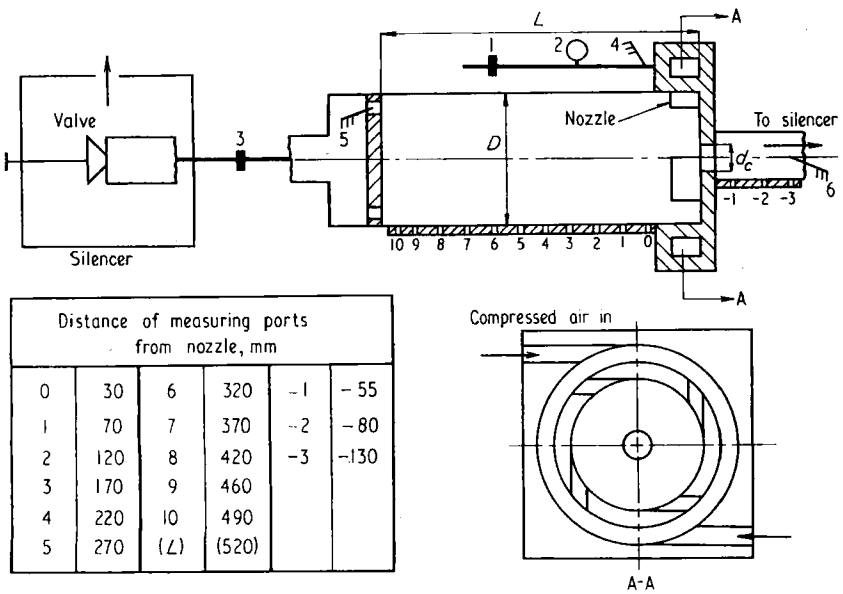

Distance of measuring ports from nozzle, mm					
0	30	6	320	-1	-55
1	70	7	370	-2	-80
2	120	8	420	-3	-130
3	170	9	460		
4	220	10	490		
5	270	(L)	(520)		

1. Venturi tube.
2. Manometer.
3. Venturi tube.
4, 5, and 6. Thermocouples.

Fig. 3. *Schematic drawing of experimental set-up*

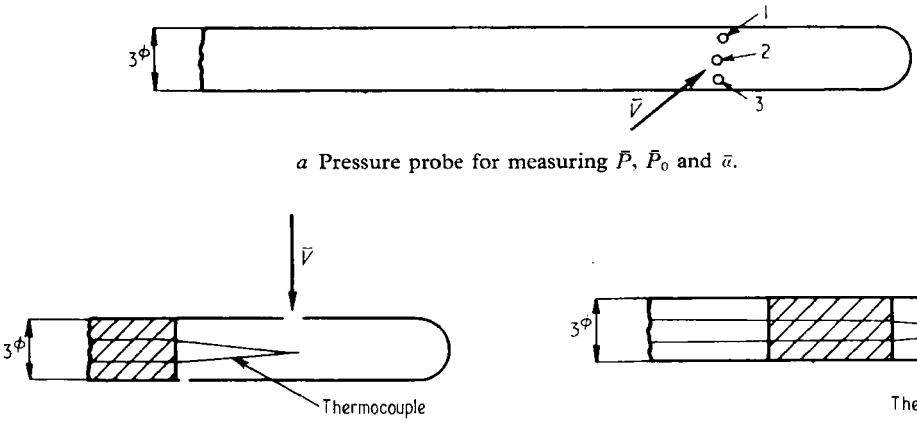

a Pressure probe for measuring $\bar{P}$, $\bar{P}_0$ and $\bar{\alpha}$.

b and *c* Temperature probes.

Fig. 4. *Probe types used for traversing the vortex tube*

calibrated in the middle of a free jet from a 20 mm nozzle.

Calibration of pressure probes

The zero position of the probe was found by rotating it in the flow until the manometers which were connected to pressure taps 1 and 3 showed the same pressure. This position was reproducible within 0·1° for velocities up to 200 m/s.

The total pressure $\bar{P}_0$ was measured by pressure tap 2 when the probe was in the zero position. When this $\bar{P}_0$ was compared with the $\bar{P}_0$ measured in the stagnation chamber of the calibration nozzle, the difference in the two $\bar{P}_0$ values was always so small that it could be explained as reading errors.

The angle β (measured from the stagnation point) which corresponds to a surface pressure equal to the static pressure $\bar{P}$ (i.e. the barometric pressure) of the main flow was measured as a function of the jet velocity calculated from the equations of subsonic flow. The angle β (approximately 45°) was constant for velocities under 100 m/s. Above 100 m/s β increased slightly with increase in velocity, and at 200 m/s β had increased by about 2° for both pressure taps 1 and 3. Repeated measurements showed that the reproducibility of the angle β for each pressure tap was within 0·1° at all velocities up to 200 m/s.

Calibration of temperature probes

The calibration of the temperature probes involved the determination of the correction factor K of the two probes *b* and *c* in Fig. 4.

The correction factor K is defined as:

$$K = \frac{\bar{T}_P - \bar{T}}{\bar{T}_0 - \bar{T}} \quad . \quad . \quad . \quad . \quad (1)$$

where $\bar{T}_0$ is the total temperature, $\bar{T}_P$ the temperature indicated by the thermocouple and $\bar{T}$ is the temperature calculated from the equations of subsonic flow. The value of $\bar{T}_P$ is due to boundary layer effects, stem conduction, radiation etc. and is extended in this report to include the deviation of the electromotive force of the thermocouple from the standard values.

The correction factors for both types of probe were found to be very close to unity. For velocities above 120 m/s the correction factors for the two types *b* and *c* were nearly constant, and had the values of 0·95 and 1·00 respectively.

Experimental procedure

The experiments were carried out with an inlet pressure $P_e = 2$ bar, an inlet temperature $T_e = 21$°C and a mass ratio $\xi = 0{\cdot}23$. When equilibrium was obtained in the vortex tube, measurements in a cross-section were undertaken with the pressure and temperature probes, and at each radial test point the quantities m_e, m_h, T_e, T_h and T_c were also measured.

The indicated flow angle $\bar{\alpha}_i$ was determined at each radial test point by means of the pressure probe (Fig. 4*a*). The probe was turned in the flow until the two mercury U-tube manometers, which were connected to pressure taps 1 and 3, showed nearly the same pressure. These manometers were then replaced by a water U-tube manometer for fine adjustment of $\bar{\alpha}_i$. This procedure allowed a determination of $\bar{\alpha}_i$ within $\pm 0{\cdot}1$°. When the probe was aligned in the flow (the zero position) the indicated total pressure $\bar{P}_{0i}$ was measured by pressure tap 2.

Since the velocity of the flow in the vortex tube was unknown the static pressure could not be measured directly because the angle β, which corresponds to the static pressure, is a function of the velocity. The variation of β found in the jet is, however, small, and it was experimentally found that a traverse with an assumed β distribution followed by a correction, was sufficient to determine the corresponding β distribution ($\beta = f(r)$) in a cross-section. Knowing this variation the indicated static pressure $\bar{P}_i$ was measured with both pressure taps 1 and 3.

Each traverse with a pressure probe was followed by measurements with temperature probes *b* and *c*. These

measurements were carried out in the cross-sections 0, 1, 2, 3, 5, 8 and 10 in the vortex tube and in the cross-section −3 in the cold outlet pipe.

To check the reproducibility of the measurements the test period was extended over several months so that it can be assumed that most of the systematic errors due to the surroundings were eliminated.

Results

The results obtained by traversing the vortex tube are shown in Figs 5–7 and in Table 1.

The indicated total pressure $\bar{P}_{0i}$ (Fig. 5), has been plotted as $\bar{P}_{0i}-P_b$ to eliminate the influence of changes in the barometric pressure P_b, when comparing repeated measurements. The same procedure has been used in plotting the indicated static pressure $\bar{P}_i$ (Fig. 6), but in this figure the curves are drawn at intervals of 50 mmHg as the slope of the curves are used for calculating the tangential velocity distribution. The ordinate on the figure therefore only corresponds to the pressure distribution in cross-section 1.

Table 1. *Radial variation of the indicated flow angle $\bar{\alpha}_i$ in six cross-sections*

r/R	Cross-sections					
	1	2	3	5	8	10
0·978	76·1	76·2	75·5	75·5	77·8	78·4
0·957	76·5	76·8	76·0	76·0	78·0	78·3
0·893	81·0	79·3	78·2	78·3	79·0	79·9
0·787	86·5	85·5	84·5	83·8	83·7	84·3
0·681	91·5	91·5	90·8	90·0	88·5	88·0
0·577	93·7	95·2	95·3	94·8	93·5	91·7
0·468	94·1	96·5	96·0	96·2	94·9	93·0
0·362	92·8	93·5	91·9	92·8	92·5	94·0
0·255	92·3	90·5	90·0	89·8	88·0	93·7
0·149	93·0	90·8	89·5	89·3	86·2	94·7
0·043	95	92	93	94	95	97

The axial variation of the static pressure (Fig. 6) is seen to be small, while a considerable decrease in the total pressure (Fig. 5) occurs in the outer layers as the flow moves down the tube.

The temperature distribution shown in Fig. 7 has been given as the total temperature. The indicated total temperature $\bar{T}_{0i}$ was calculated from the probe temperature $\bar{T}_P$ by using the correction factor K and the Mach number calculated from $\bar{P}_{0i}$ and $\bar{P}_i$. Fig. 7 thus shows the indicated total temperature $\bar{T}_{0i}$ plotted as $\bar{T}_{0i}-\bar{T}_e$. For comparison the total temperature distribution in cross-section −3 in the cold outlet pipe is also plotted. Inserting a probe in the vortex tube changes the temperature distribution in the cold outlet pipe. Therefore two curves have been drawn in Fig. 7; the curve −3a shows the total temperature distribution in the cold outlet pipe without any probes in the vortex tube, while the curve −3b shows the total temperature distribution in the cold outlet pipe with a pressure or temperature probe inserted 30 to 40 mm into the vortex tube in any of the cross-sections 1 to 10.

The curves show that the whole temperature level changes from cross-section to cross-section. As the flow moves down the tube the total temperature approaches the temperature of the hot air $\bar{T}_h$ and the indicated total temperature $\bar{T}_{0i}$ in the outer layers of cross-section 10 deviates less than 1 degC from $\bar{T}_h$. Similarly, the total

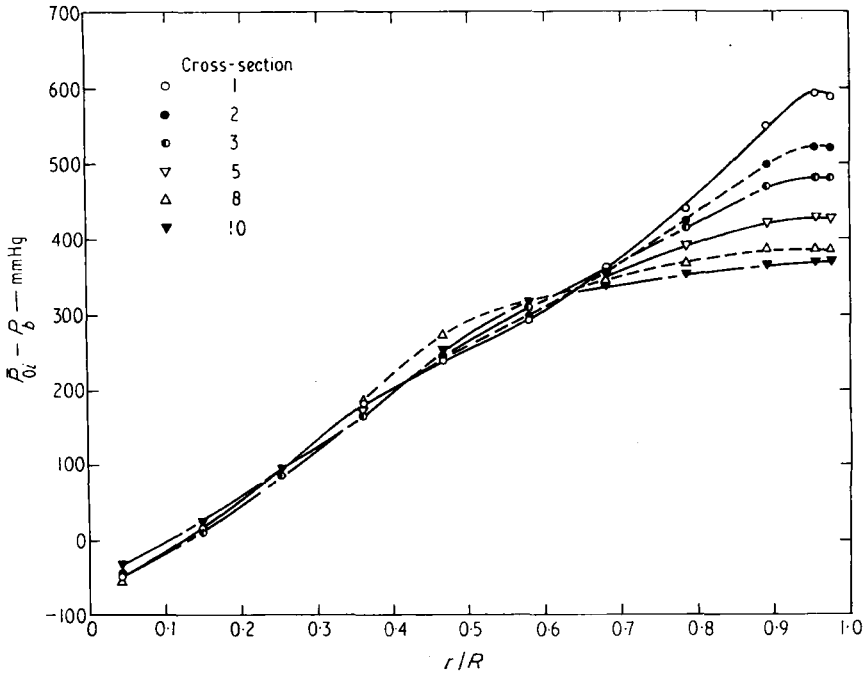

P_b = barometric pressure.

Fig. 5. *Distribution of indicated total pressure $\bar{P}_{0i}$ in six cross-sections*

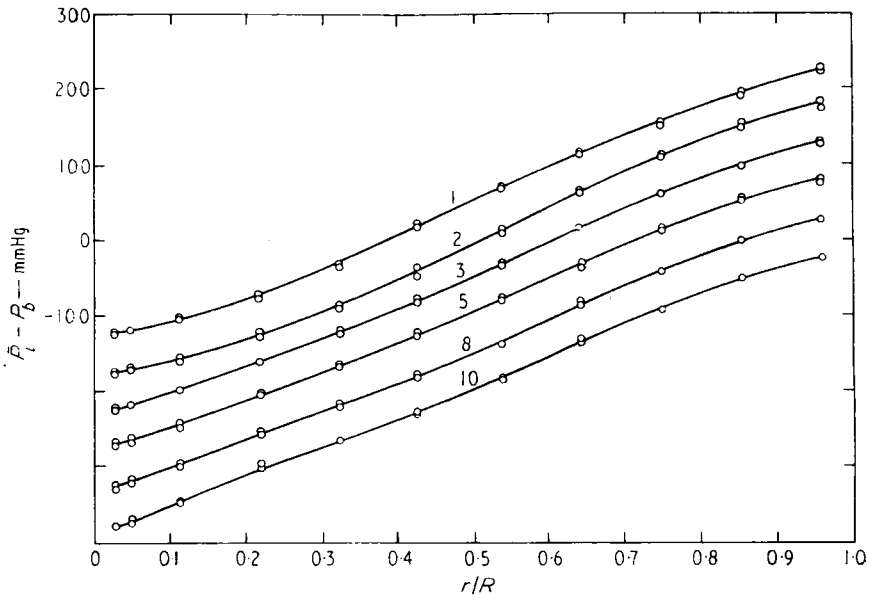

P_b = barometric pressure. The pressure scale only refers to curve 1; the other curves are drawn at 50 mmHg intervals.

Fig. 6. *Distribution of indicated static pressure $\bar{P}_i$ in six cross-sections*

temperature distribution in the central and medium layers of a cross-section approaches the temperature distribution in the cold outlet pipe as the back flow moves towards the cold orifice.

Since the radial component of the velocity $\bar{u}$ is very small, the direction of the main flow can be described by the angle $\bar{\alpha}$ between the velocity vector and the axial direction. The flow angle $\bar{\alpha}$ is defined so that the value zero corresponds to purely axial flow directed towards the hot outlet. To emphasize the small but important axial variation the indicated flow angle $\bar{\alpha}_i$ is given in tabular form (Table 1). In the table the mean values of repeated measurements of the flow angle $\bar{\alpha}_i$ are given as functions of r/R for six cross-sections.

The results for the cold outlet pipe were found to be similar to the results for the vortex tube, except that the gradients were much smaller.

The accuracy of the measurements depends on random errors due to uncertainties in calibration, reading errors, etc., and on fixed errors which are mainly due to turbulence and flow disturbance caused by the probes. The uncertainty in the flow quantities due to the random errors were found both by calculation and from the scatter in the results to be: $\bar{\alpha}_i$: $\pm 0{\cdot}2°$; $\bar{P}_{0i}$: ± 2 mmHg; $\bar{P}_i$: ± 4 mmHg; and $\bar{T}_{0i}$: $\pm 0{\cdot}25$ degC.

The magnitude of the fixed errors due to turbulence and flow disturbance were investigated in various ways.

The influence of *turbulence* on the measurements of the indicated flow angle $\bar{\alpha}_i$ was small due to the symmetry of the pressure probe. The effect on the indicated total temperature $\bar{T}_{0i}$ is also small, as the equation relating temperature and total temperature

$$c_p T_0 = c_p T + \tfrac{1}{2}\bar{V}^2 \quad . \quad . \quad . \quad (2)$$

after substituting mean values and fluctuations and averaging with respect to time, is still valid within a few per cent for the mean values alone, even at a turbulence intensity of 0·1. The influence on the pressure measurements can, however, be considerable.

A check on this fixed error in the static pressure was obtained by comparing the static pressure measured with pressure taps placed on the surface of the vortex tube and the static pressure measured 1 mm inside the vortex tube with the pressure probe (Fig. 4*a*). The results of this are shown in Fig. 8, where a difference of 40 to 70 mmHg occurs between the two curves. As shown later, the effect of this error on the determination of the velocity can be compensated to a large extent.

The fixed errors due to *flow disturbance* caused by the probes were investigated in the following ways.

Changes in the static pressure

The static pressure $\bar{P}_{r=R}$ along the length of the surface of the vortex tube was measured by pressure tappings from ports 1 to 10. The change in $\bar{P}_{r=R}$ with a probe in the outer layers of one of the cross-sections 1 to 10 was small.

When the probe crossed the interface between the oppositely directed axial flows (see later) $\bar{P}_{r=R}$ started to decrease and dropped about 25 mmHg when the probe was inserted 30 to 40 mm. The insertion therefore causes only a small change in the velocity $\bar{V}$ and the tangential velocity component $\bar{v}$ in the central part of the vortex tube.

Changes in the flow angle

The variation in $\bar{\alpha}$ due to flow disturbance was indicated by the variation in the mass ratio ξ with the radial position

of the probe (Fig. 9). The curves which are drawn at 0·02 intervals show that the variation is nearly the same in all cross-sections, and that the total variation in ξ is only about 0·03. In the outer and medium layers of the vortex tube the measured $\bar{\alpha}_i$ values will therefore be very close to the real $\bar{\alpha}$ values, while a greater difference exists in the central part.

Changes in the total temperature

To examine the influence of the radial position of the probe on the total temperature distribution, investigations of the change in T_{ci} and T_h were carried out. The variation for the temperature drop $\Delta T_{ci} = T_e - T_{ci}$ is shown in Fig. 10. The curves, which are drawn 2 degC apart, show that the variation is nearly the same in all cross-sections. Probes in the outer layers have very little influence on the temperature drop ΔT_{ci}. When the probe tip is close to the interface (shown by a dash) there is a change in ΔT_{ci} which drops 4 to 6 degC within a traverse of about 10 mm; further in, ΔT_{ci} has a constant, but lower, value.

It can therefore be concluded that the measured temperature $\bar{T}_{0i}$ in the outer layers is very close to the total temperature $\bar{T}_0$. In the medium layers, close to the interface, a small deviation exists and in the central part $\bar{T}_{0i}$ is about 5 degC higher than the total temperature $\bar{T}_0$.

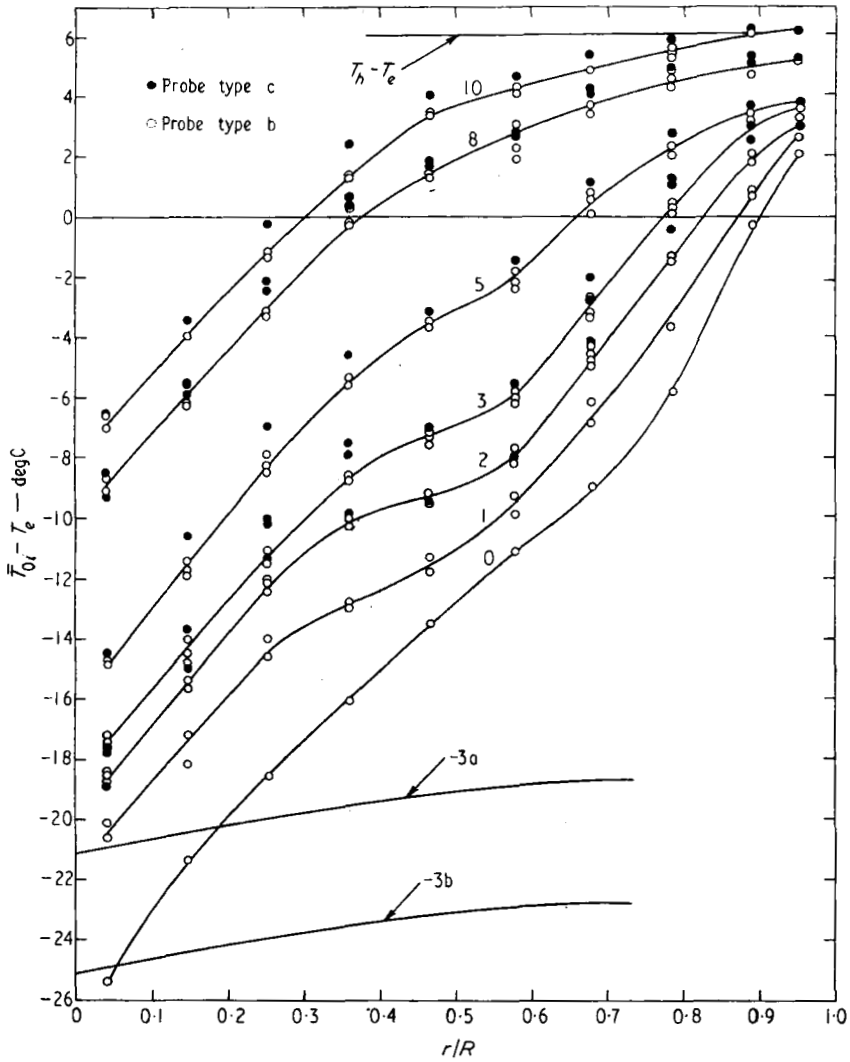

Curve −3a shows the total temperature measured in the cold outlet pipe without any probes in the vortex tube; curve −3b with a probe inserted 30 to 40 mm in any of the cross-sections 1 to 10.

Fig. 7. *Distribution of indicated total temperature $\bar{T}_{0i}$ in six cross-sections in the vortex tube and one cross-section (−3) in the cold outlet pipe*

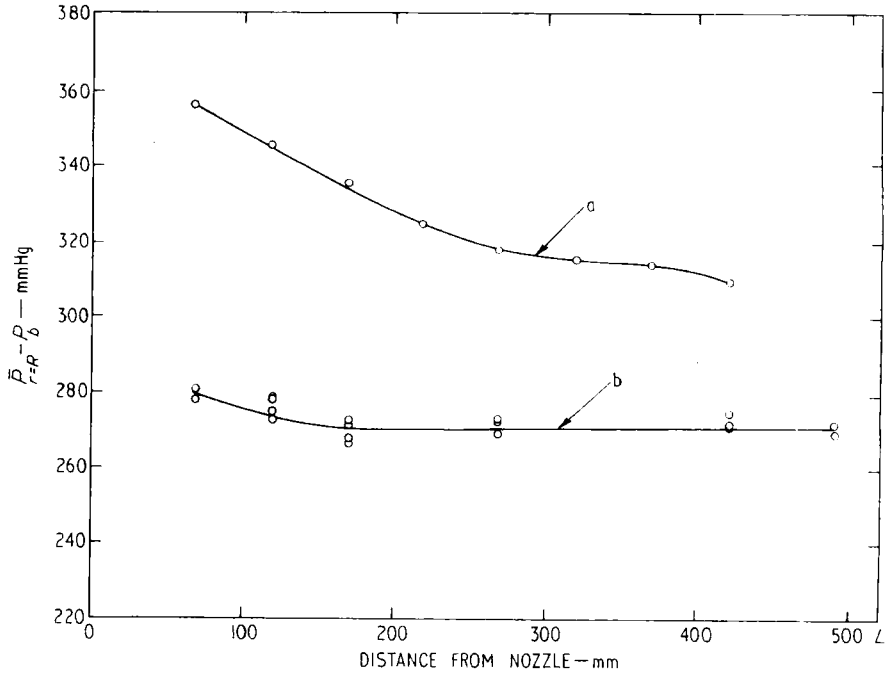

Curve a is measured with pressure taps in the tube wall, curve b with the pressure taps of the pressure probe 1 mm inside the vortex tube.

Fig. 8. *Static pressure at the tube wall*

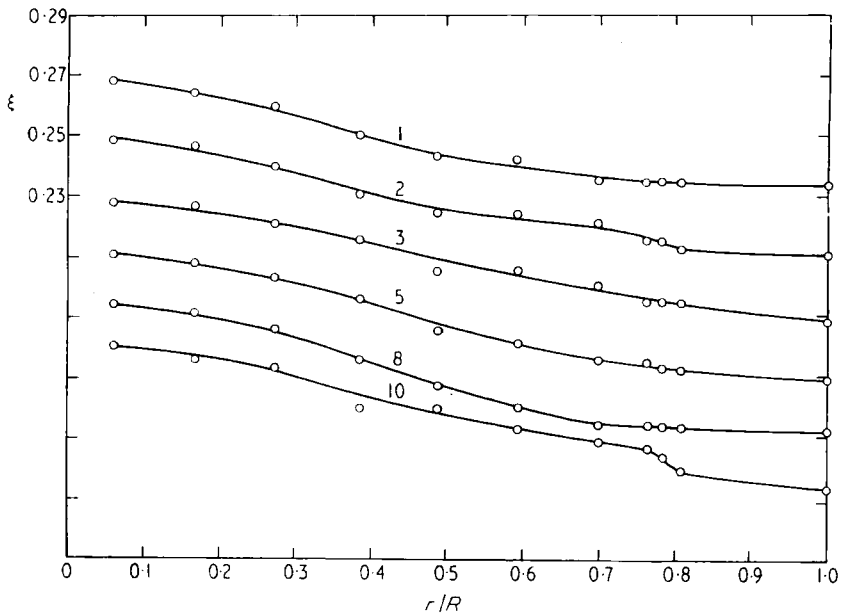

The ordinate refers to curve 1; other curves are drawn at 0·02 intervals.

Fig. 9. *Variation in the mass ratio ξ with radial position of the probe tip in six cross-sections*

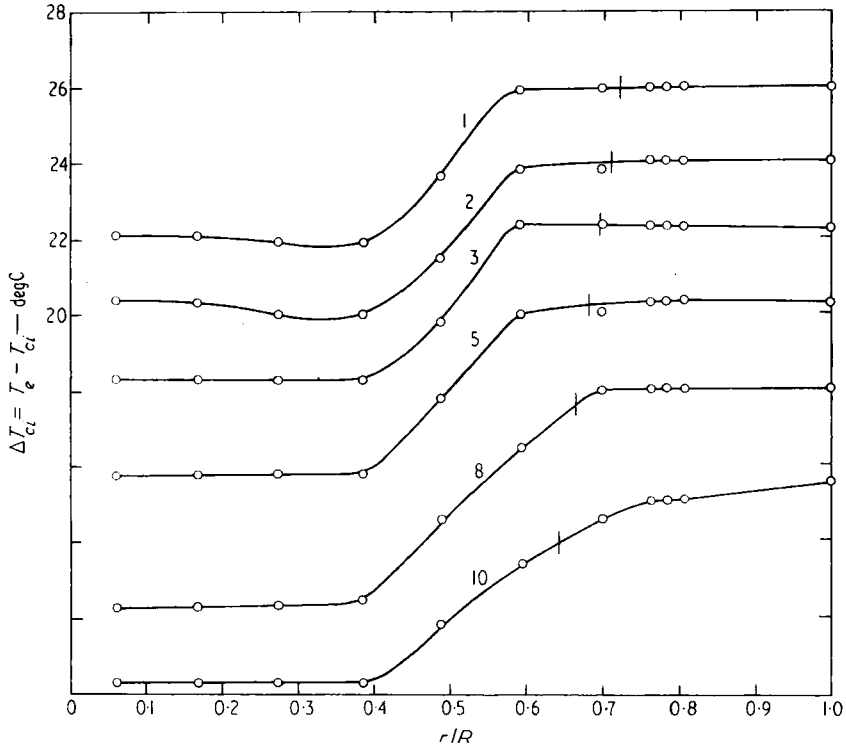

The dashes on the curves indicate the position of the interface. The ordinate refers to curve 1; the other curves are drawn at 2 degC intervals.

Fig. 10. *Variation in ΔT_{ci} with radial position of probe tip in six cross-sections*

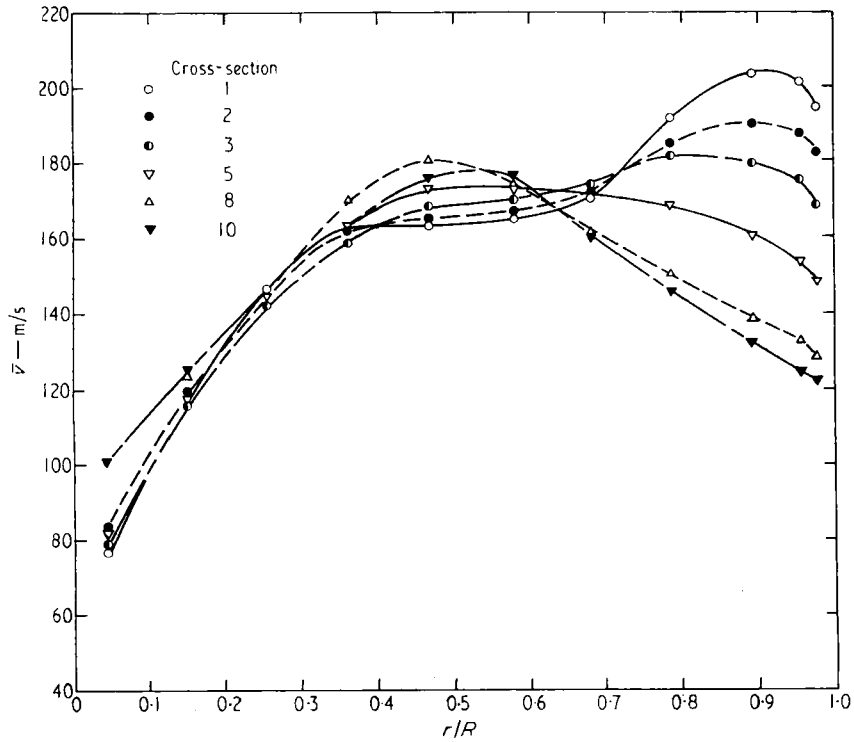

Fig. 11. *The tangential velocity distribution in six cross-sections calculated from $\bar{P}_{0i}$, $\bar{P}_i$, $\bar{T}_{0i}$ and $\bar{\alpha}_i$*

CALCULATIONS

Tangential and axial velocity components

Using the ordinary equation of subsonic flow the tangential and axial velocity components $\bar{v}$ and $\bar{w}$ can be calculated from the measured $\bar{P}_i$, $\bar{P}_{0i}$, $\bar{T}_{0i}$ and $\bar{\alpha}_i$ values. The results of these calculations are shown in Figs 11 and 13 for the vortex tube and in curves a and b in Fig. 15 for the cold outlet pipe.

The tangential and axial velocity distribution can also be calculated from the slope of the static pressure curves, the density $\bar{\rho}$ and the $\bar{\alpha}_i$ values. As can be shown, the radial equation of motion (apart from the boundary layer close to the tube wall) reduces to

$$\frac{\partial \bar{P}}{\partial r} = \bar{\rho}\frac{\bar{v}^2}{r} \quad . \quad . \quad . \quad . \quad . \quad (3)$$

The exact value of $\partial \bar{P}/\partial r$ is not known, but as the fixed error of the static pressure $\bar{P}-\bar{P}_i$ is of the same order of magnitude at all radii in a cross-section, the $\bar{P}$ and $\bar{P}_i$ curves are nearly parallel. The deviation between $\partial \bar{P}/\partial r$ and $\partial \bar{P}_i/\partial r$ in the main part of the vortex tube is therefore small, and the tangential velocity component can be calculated from

$$\bar{v} = \sqrt{\frac{r}{\bar{\rho}}\frac{\partial \bar{P}_i}{\partial r}} \quad . \quad . \quad . \quad . \quad (4)$$

From this tangential velocity the corresponding axial velocity can be calculated as $\bar{w} = \bar{v}\cot\bar{\alpha}_i$.

The results of these calculations are shown in Figs 12 and 14 for the vortex tube and in curves c and d in Fig. 15 for the cold outlet pipe.

Figs 11 and 12 show that the two sets of curves are similar when calculated by the two methods but are displaced in terms of absolute values. In Fig. 11 the values of $\bar{v}$ for $r/R < 0{\cdot}3$ (which are nearly the same for all cross-sections) are all 30 to 40 m/s higher than the corresponding values in Fig. 12. In the medium layers the corresponding values are 15 to 20 m/s higher and in the outer layers ($r/R > 0{\cdot}6$) the difference in cross-sections 1 to 5 is 20 to 30 m/s, while in cross-sections 8 and 10 the difference is less than 5 m/s.

The accuracy of the two methods was checked by calculating the mass flows from the two axial velocity distributions in the vortex tube (Figs 13 and 14) and in the cold outlet pipe (curves b and d in Fig. 15) respectively, and comparing them with the venturi tube measurements. According to the equation of continuity, the mass flow through a cross-section in the vortex tube is equal to the hot mass flow m_h, while the mass flow through a cross-section in the cold outlet pipe is equal to the cold mass flow m_c.

Calculations based on the axial velocity distribution in Fig. 13 gave values of the hot mass flow varying from 0·082 kg/s to 0·118 kg/s, while the calculations based on the axial velocity distribution in Fig. 14 gave the hot mass flows shown in Table 2.

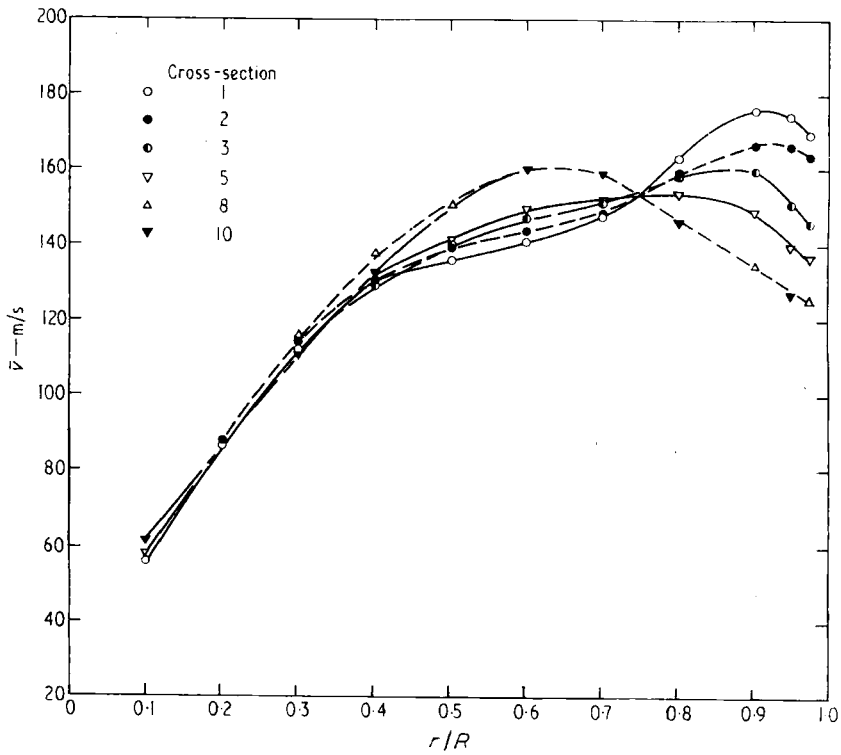

Fig. 12. *The tangential velocity distribution in six cross-sections calculated from* $\partial \bar{P}_i/\partial r$

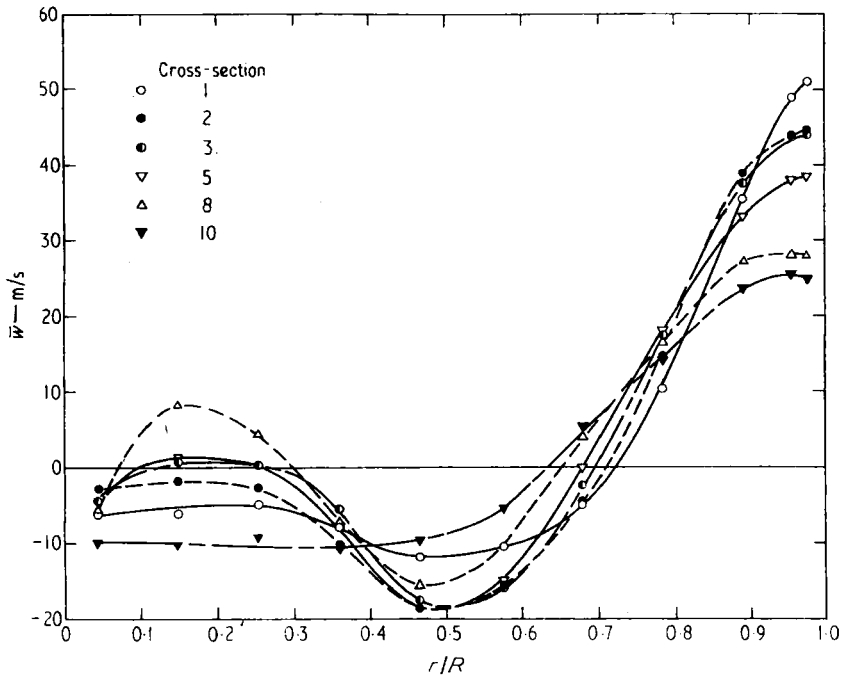

Fig. 13. *The axial velocity distribution in six cross-sections calculated from* $\bar{P}_{0i}$, $\bar{P}_i$, $\bar{T}_{0i}$ *and* $\bar{\alpha}_i$

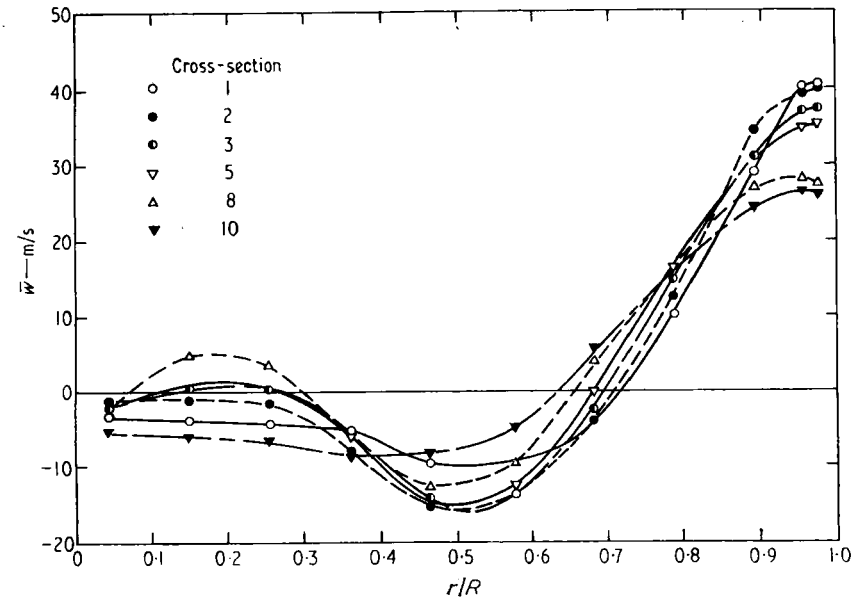

Fig. 14. *The axial velocity distribution in six cross-sections calculated from* $\partial\bar{P}_i/\partial r$ *and* $\bar{\alpha}_i$

Table 2. *Hot mass flow*

	Mass flow, kg/s
Venturi tube measurements	0·094
Integration (Fig. 14):	
Cross-section: 1	0·099
2	0·097
3	0·098
5	0·098
8	0·097
10	0·093

Table 3. *Cold mass flow*

	Mass flow, kg/s
Venturi tube measurements	0·028
Integration (Fig. 15):	
Curve b	0·041
Curve d	0·033

In the same way the calculations for the cold outlet pipe gave the values shown in Table 3.

Since the integrated mass flows for the vortex tube and the cold outlet pipe give values close to the venturi tube measurements, when the velocity distribution, based on the slope of the pressure curves and the $\bar{\alpha}_i$ values is used, it can be concluded that the actual velocity distribution in the vortex tube and in the cold outlet pipe must be close to the velocity distribution shown in Figs 12 and 14 and in curves c and d in Fig. 15 respectively.

From the axial velocity distribution in the cold outlet pipe (curve d, Fig. 15) it is seen that there exists a back flow in the central part. The configuration of this pipe will therefore affect the flow in the vortex tube.

Curve 1 in Fig. 12 shows that the tangential velocity distribution in the central and medium layers of cross-section 1 near the nozzle section is of the forced vortex type ($\bar{v} \sim r^n$, $n \sim 1$). As the wall is approached the velocity distribution in the outer layers changes and becomes of the free vortex type ($\bar{v} \sim r^m$, $m \sim -1$) close to the wall.

As the flow moves down the tube the maximum tangential velocity and the velocity in the outer layers decreases, while the velocity in the medium layers increases. The free vortex will thus 'grow' towards the medium layers as the flow progresses down the tube.

Fig. 14 shows that the axial velocity in the outer layers is

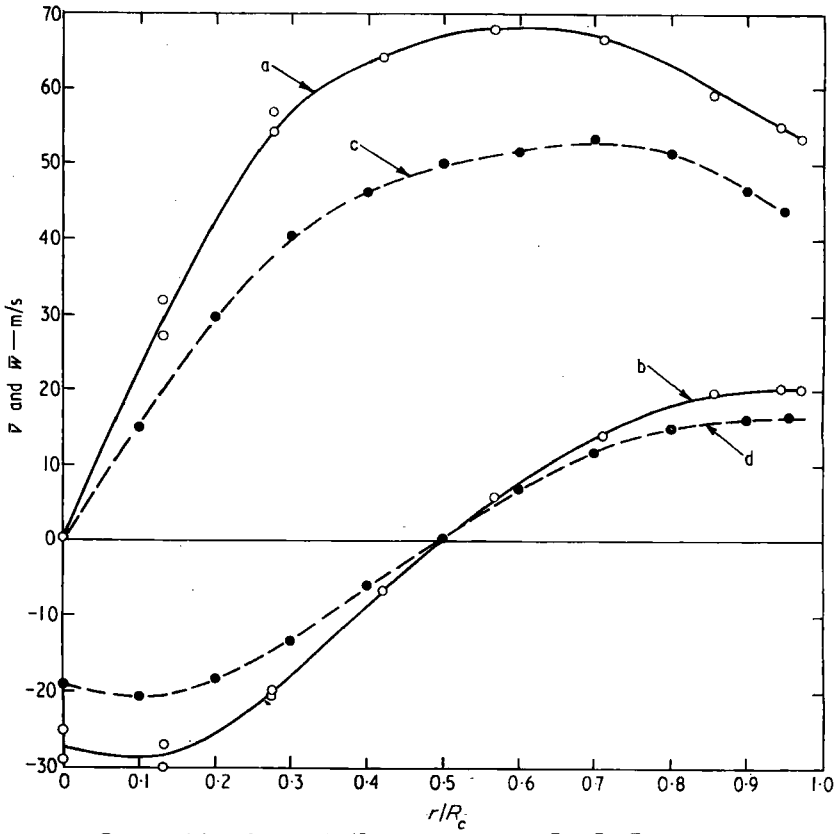

Curve a ($\bar{v}$) and curve b ($\bar{w}$) calculated from $\bar{P}_{0i}$, $\bar{P}_t$, $\bar{T}_{0i}$, and $\bar{\alpha}_i$.
Curve c ($\bar{v}$) and curve d ($\bar{w}$) calculated from $\partial \bar{P}_t/\partial r$ and $\bar{\alpha}_i$.

Fig. 15. *Tangential ($\bar{v}$) and axial ($\bar{w}$) velocity distribution in cross-section —3 in the cold outlet pipe*

directed towards the hot outlet and that the greatest axial velocity is found close to the tube wall. The axial velocity in medium layers is directed towards the cold outlet, while the direction of the axial velocity in the central part depends on the axial position of the cross-section.

As the flow progresses down the tube the maximum axial velocity decreases, and the interface between the oppositely directed axial velocities moves inwards.

The same tangential and axial velocity distribution has in principle been found by Eckert and Hartnett (**2**), Lay (**3**) and Takahama and Kawashima (**4**) in different types of uniflow and counterflow vortex tubes. The somewhat different tangential velocity distribution found by Reynolds (**5**) can, according to the experiments carried out by Eckert and Hartnett, be explained by the use of a *central* hot outlet.

Radial velocity distribution

The radial velocity component $\bar{u}$ was calculated from the equation of continuity. As the flow is rotational symmetric and has steady mean values the equation of continuity can be reduced to

$$\frac{\partial(r\bar{\rho}\bar{u})}{\partial r}+\frac{\partial(r\bar{\rho}\bar{w})}{\partial z}=0 \quad . \quad . \quad . \quad (5)$$

without deviating more than a few per cent from the complete turbulent equation of continuity.

Integrating equation (5) with respect to r the equation becomes

$$r\bar{\rho}\bar{u}=-\int_0^r \frac{\partial(\bar{\rho}\bar{w})}{\partial z} r\,\mathrm{d}r \quad . \quad . \quad . \quad (6)$$

An approximate solution of the real radial velocity distribution $\bar{u}$ was obtained by numerical integration of equation (6). As the axial variation of the density $\bar{\rho}$ was very small $\partial(\bar{\rho}\bar{w})/\partial z$ was replaced by $\bar{\rho}(\partial\bar{w})/(\partial z)$, and the value of $(\partial\bar{w})/(\partial z)$ approximated by $\Delta\bar{w}_{ab}/\Delta z_{ab}$, where $\Delta\bar{w}_{ab}$ is the change in the $\bar{w}$ value (Fig. 14) from cross-section a to cross-section b and Δz_{ab} is the corresponding distance. This procedure gives the axial mean values of the radial velocity $\bar{u}_{ab}$ between cross-sections a and b. The values of $\bar{u}_{ab}$ as functions of r/R for ab = 1 2, 2 3, 3 5, 5 8 and 8 10 are shown in Fig. 16.

The radial velocity on the interface between the oppositely directed axial velocities was checked by calculating the change in the mass flows on the two sides of the interface. The mass flows on the two sides of the interface in cross-section a is denoted as the cold mass flow m_{ca} and the hot mass flow m_{ha} respectively. The radial velocity on the interface $\bar{u}_{ab}(r_e)$ was calculated from the change in the hot and cold mass flows $\Delta m_h = m_{hb}-m_{ha}$ and $\Delta m_c = m_{cb}-m_{ca}$. According to the equation of continuity, calculations based on Δm_c, Δm_h and equation (6) respectively should give the same values of $\bar{u}_{ab}(r_e)$. The results of these calculations are shown in Table 4.

Table 4 shows that there exists an outwardly directed radial velocity $\bar{u}$ between the nozzle section and cross-section 2. The radial velocity $\bar{u}_{ab}(r_e)$ is directed inwards in the rest of the vortex tube and as the hot mass flow in cross-section 10 is considerably greater than m_h, a relatively large inward mass flow must occur near the hot outlet.

The outwardly directed radial velocity near the nozzle

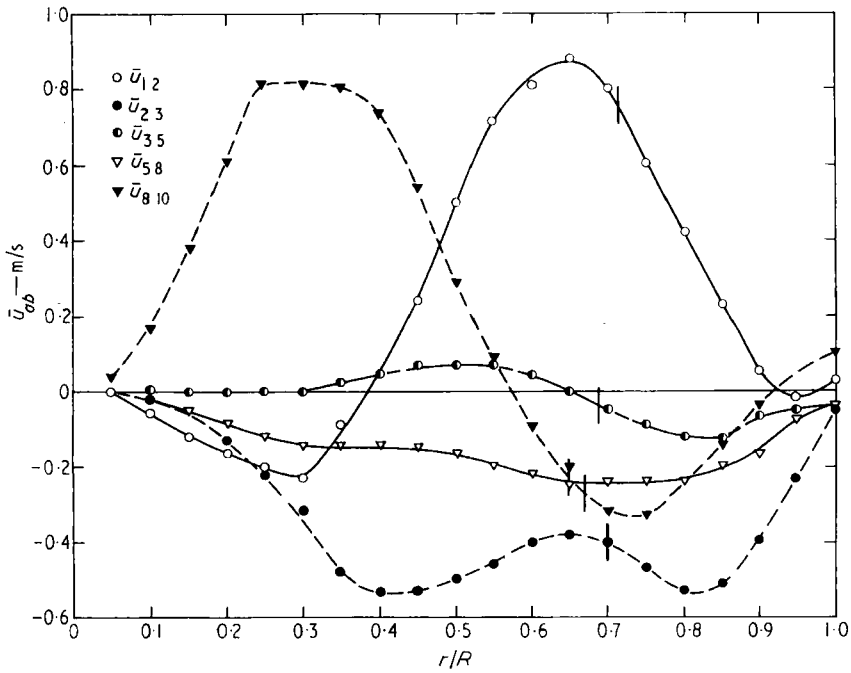

Fig. 16. *The axial mean values of the radial velocity $\bar{u}_{ab}$ between six cross-sections*

Table 4. *The axial mean values of the radial velocity $\bar{u}_{ab}$ on the interface*

	Mass flows		Radial velocity $\bar{u}_{ab}(r_e)$ calculated from:		
	m_{ca}, kg/s	m_{ha}, kg/s	(6), m/s	(m_c), m/s	(m_h), m/s
Cold outlet (m_c)	0·028			$\bar{u} > 0$	
Cross-section 1	0·034	0·133	+0·74	+0·73	+0·61
2	0·046	0·143	−0·41	−0·43	−0·37
3	0·039	0·137	−0·04	−0·03	−0·03
5	0·038	0·136	−0·25	−0·24	−0·26
8	0·027	0·124	−0·20	−0·20	−0·40
10	0·023	0·116			$\bar{u} < 0$
Hot outlet (m_h)		0·094			

section is not in accordance with the earlier assumptions. The only experimental indication of this radial velocity distribution was found by visual investigation by Scheper (6), using silk threads. But by performing the same calculations as used above on the results obtained by Eckert and Hartnett (2) and Lay (3) the same type of radial velocity distribution was found.

Temperature distribution

The temperature distribution (Fig. 17) was calculated from the total temperature distribution (Fig. 7) and the tangential and axial velocity distributions (Figs 12 and 14).

As the disturbance of the total temperature caused by the probes was rather large in the central part of the vortex tube, the temperature $\bar{T}$ was only calculated for $r/R > 0{\cdot}5$, and $\bar{T}$ in the medium layers has been corrected for the flow disturbance shown in Fig. 10.

A similar temperature distribution was found when the velocity distributions in Figs 11 and 13 were used for

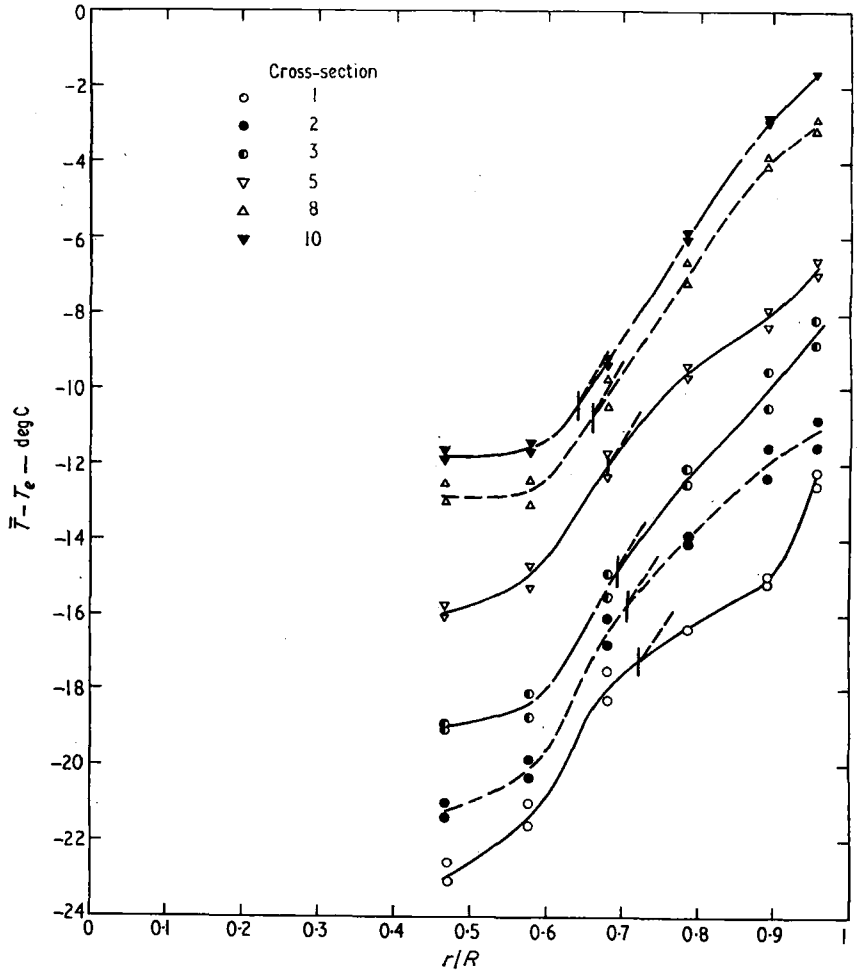

The dashed lines indicate the slope of an adiabatic temperature distribution at the interface.

Fig. 17. *Temperature distribution in six cross-sections calculated from the velocity distributions in Figs 12 and 14*

calculating the temperature $\bar{T}$ except that the corresponding curves for cross-sections 1 to 5 were displaced about 3 degC.

The slope of the adiabatic expansion corresponding to the pressure distribution $\bar{P} = f(r, z)$ in the vortex tube, can be calculated from

$$\frac{\partial \bar{T}_{ad}}{\partial r/R} = \frac{\gamma-1}{\gamma}\frac{\bar{T}}{\bar{P}}\frac{\partial \bar{P}}{\partial r/R} \quad . \quad . \quad . \quad (7)$$

When this equation is applied at the interface between the oppositely directed axial velocities, a value of $(\partial \bar{T}_{ad})/(\partial r/R) = 31$ degC is found in cross-sections 1 and 2 if the effect of the systematic errors are neglected. As the flow progressed down the tube the value of $(\partial \bar{T}_{ad})/(\partial r/R)$ increased and reached the value of 38 degC in cross-section 10. These slopes are drawn in Fig. 17. The figure shows that the slope of the real temperature distribution on the interface is smaller than the slope which corresponds to an adiabatic temperature distribution in all cross-sections. However, as the flow moves down the tube the temperature distribution approaches the adiabatic temperature distribution, and the difference between the two temperature distributions is seen to be small in cross-sections 8 and 10.

COMPARISON WITH OTHER WORK

The experimental results show that the velocity is predominantly tangential. The radial equation of motion can, therefore, as mentioned earlier, be written as

$$\frac{\partial \bar{P}}{\partial r} = \bar{\rho}\frac{\bar{v}^2}{r} \quad . \quad . \quad . \quad . \quad . \quad . \quad (8)$$

When the magnitude of the two terms in this equation is compared with the convection terms in the tangential and axial equations of motion, it is found that these convection terms are only about the order of 1/100 of the terms in equation (8). The main flow in the vortex tube can therefore be described by equation (8) alone with a good degree of approximation.

In the first attempts to solve the equations of motion for the flow in the vortex tube only the radial equation (8) was considered. When applying this equation the following flow model was assumed: the flow consisted of a forced vortex ($v \sim r$) in the central part and a free vortex ($v \sim 1/r$) in the outer part of the vortex tube. The forced vortex corresponds to the cold mass flow and the free vortex to the hot mass flow. Furthermore, the axial velocity was uniform in each flow, but in opposite directions, and the radial velocity was zero.

When this vortex model was applied to the equation of energy it was found that the convection terms vanished, so that the equation of energy was reduced to a balance between heat conduction and viscous dissipation:

$$0 = \frac{1}{r}\frac{\mathrm{d}}{\mathrm{d}r}\left(\lambda r \frac{\mathrm{d}T}{\mathrm{d}r}\right) + \mu\left(\frac{\mathrm{d}v}{\mathrm{d}r} - \frac{v}{r}\right)^2 \quad . \quad . \quad (9)$$

As the flow in the vortex tube is strongly turbulent, van Deemter (7) assumed that the effects of the laminar conductivity and viscosity are negligible compared with the corresponding turbulent quantities. He therefore replaced μ in equation (9) by a turbulent viscosity μ_t, and for the turbulent heat conduction he assumed that heat is only transported by turbulence when the temperature distribution differs from the corresponding adiabatic temperature distribution. He therefore replaced $\lambda(\mathrm{d}T/\mathrm{d}r)$ in equation (9) by $\lambda_t[(\mathrm{d}\bar{T}/\mathrm{d}r) - (\mathrm{d}\bar{T}_{ad}/\mathrm{d}r)]$. In the turbulent flow model the energy equation therefore takes the form:

$$0 = \frac{1}{r}\frac{\mathrm{d}}{\mathrm{d}r}\left[\lambda_t r\left(\frac{\mathrm{d}\bar{T}}{\mathrm{d}r} - \frac{\mathrm{d}\bar{T}_{ad}}{\mathrm{d}r}\right)\right] + \mu_t\left(\frac{\mathrm{d}\bar{v}}{\mathrm{d}r} - \frac{\bar{v}}{r}\right)^2 \quad (10)$$

where

$$\frac{\mathrm{d}\bar{T}_{ad}}{\mathrm{d}r} = \frac{\gamma-1}{\gamma}\frac{\bar{T}}{\bar{P}}\frac{\mathrm{d}\bar{P}}{\mathrm{d}r} \quad . \quad . \quad . \quad (11)$$

By substituting equations (8) and (11) into equation (10) the energy equation takes the form:

$$0 = \frac{1}{r}\frac{\mathrm{d}}{\mathrm{d}r}\left[\lambda_t r\left(\frac{\mathrm{d}\bar{T}}{\mathrm{d}r} - \frac{\bar{v}^2}{c_p r}\right)\right] + \mu_t\left(\frac{\mathrm{d}\bar{v}}{\mathrm{d}r} - \frac{\bar{v}}{r}\right)^2 \quad (12)$$

When the laminar and turbulent energy equations (9) and (12) were solved for the assumed vortex model, a variation in the total temperature $\bar{T}_0$ across the vortex was found in both cases.

However, this theory cannot explain the great change in the velocity and temperature distribution as the flow moves down the vortex tube.

Second order approaches have been carried out by Deissler and Perlmutter (8) (9) and Suzuki (10) by including the equation of continuity, the tangential equation of motion and the convection terms in the energy equation in the calculations. However, their flow models only included the radial variation and neglected the axial variation (except for the axial velocity). Therefore basically the same tangential velocity and temperature distributions were found as in the first order approximations.

However, it can be shown that the effect of the axial variation is as important as the radial variation. The convection terms in the equations of motion and in the equation of energy are of the form $\bar{u}(\partial/\partial r) + \bar{w}(\partial/\partial z)$. The experimentsl results of the author and those of Eckert and Hartnett (2) and Lay (3) show that $\bar{u} \simeq 1$ m/s and $\bar{w} \simeq 10$–20 m/s. As $\partial/\partial z$ is one-tenth of $\partial/\partial r$ for $\bar{v}$, $\bar{w}$ and $\bar{T}$, the two terms $\bar{u}(\partial/\partial r)$ and $\bar{w}(\partial/\partial z)$ are of the same order of magnitude in both the equations of motion and energy. A second-order approximation must therefore include the axial variation as well as the radial variation. In such an approach the equations become very difficult to solve, but it is still possible to give a physical description of the most important factors in the energy separation.

By re-writing the energy equation in terms of the total temperature and by introducing mean values and fluctuations Bruun (11) has shown that the energy equation can be reduced to

$$\bar{\rho}c_p\left(\bar{u}\frac{\partial \bar{T}_0}{\partial r} + \bar{w}\frac{\partial \bar{T}_0}{\partial z}\right) = \underbrace{-\frac{\bar{v}}{r^2}\frac{\partial(r^2\bar{\rho}\overline{v'u'})}{\partial r}}_{(A)} \underbrace{-\frac{1}{r}\frac{\partial(rc_p\bar{\rho}\overline{u'T'})}{\partial r}}_{(B)} \quad . \quad . \quad . \quad (13)$$

where term (A) involves the turbulent tangential Reynolds stress

$$\bar{\rho}\overline{u'v'} \simeq -\mu_t\left(\frac{\partial\bar{v}}{\partial r}-\frac{\bar{v}}{r}\right) \quad . \quad . \quad . \quad (14)$$

and term (B) involves the turbulent heat transfer

$$\bar{\rho}c_p\overline{u'T'} \simeq -\lambda_t\left(\frac{\partial\bar{T}}{\partial r}-\frac{\mathrm{d}\bar{T}_{ad}}{\partial r}\right) \quad . \quad . \quad (15)$$

according to van Deemter (7).

From the relations (14) and (15), the influence of terms (A) and (B) on the separation effect can be evaluated. As the tangential velocity distribution near the inlet is nearly a forced vortex, the turbulent Reynolds stress will nearly be zero and thus term (A) ~ 0. On the other hand, the temperature distribution differs considerably from the adiabatic temperature distribution in this part of the vortex tube (Fig. 17). The term (B) will therefore be the predominant term in this part of the vortex tube. At the other end of the vortex tube it is seen from Fig. 7 that $\bar{T}_0$ approaches a constant value across the vortex tube, and Takahama and Kawashima (4) show that $\bar{T}_0$ becomes constant over the cross-section when the cross-section is located beyond the optimum length (L_{opt}) of the vortex tube. Furthermore, Metenin (12) has shown that the change in separation effect with increasing length L of the vortex tube is very small when $L > L_{opt}$. From these results it follows that in this part of the vortex tube both the radial and axial convection terms in the energy equation (13) are very small. As the temperature distribution in this part of the vortex tube is nearly adiabatic, the term (B) will also be very small and to satisfy equation (13) term (A) must also be very small. As the flow is a free vortex in the outer part and thus $\overline{u'v'} \neq 0$, the only way this can be obtained is by having a much small ratio of μ_t/μ than for a plane flow where the ratio may be as high as 1·000 to 10·000.

From these considerations it can therefore be concluded that the major contribution to the energy separation is from the turbulent heat transport.

CONCLUSIONS

From the measured and calculated quantities, it is seen that the flow and the energy separation in the vortex tube cannot be described by a simple flow model. The results have clearly demonstrated that the axial variation cannot be neglected compared with the radial variation since the radial velocity $\bar{u}$ is small compared with the axial velocity $\bar{w}$. Furthermore the calculations of the radial velocity distribution have shown that an outwardly directed radial velocity exists near the nozzle section.

From the turbulent energy equation (13) it can be concluded that the energy separation is mainly caused by adiabatic contraction and expansion of turbulent eddies in a centrifugal field with a non-adiabatic temperature distribution and a radial variation of the axial velocity $\bar{w}$.

ACKNOWLEDGEMENTS

The author wishes to express his thanks to Professor K. Refslund and Dr H. Saustrup Christensen (Technical University of Denmark, Department of Fluid Mechanics), Professor G. M. Lilley (University of Southampton, Department of Aeronautics) and Dr P. O. A. L. Davies (University of Southampton, Institute of Sound and Vibration Research) for advice.

APPENDIX

REFERENCES

(1) RANQUE, G. J. 'Expériences sur la détente giratoire avec productions simultanées d'un échappement d'air chaud et d'un échappement d'air froid', *J. Phys. Radium* 1933 **4** (Series VII, June, No. 6) (No. 342, *Bulletin Bi-mensual*), 112S.

(2) ECKERT, E. R. G. and HARTNETT, J. P. 'Experimental study of the velocity and temperature distribution in a high velocity vortex flow', *Trans. Am. Soc. mech. Engrs* 1957 **79** (May), 751.

(3) LAY, J. E. 'An experimental and analytical study of vortex flow temperature separation by superposition of spiral and axial flow. Part 1', *J. Heat Transfer, Trans. Am. Soc. mech. Engrs* 1959 **81** (Series C, No. 3, August), 202.

(4) TAKAHAMA, H. and KAWASHIMA, K. I. 'An experimental study of vortex tubes', *Mem. Fac. Engng Nagoya Univ.* 1960 **12**, 227.

(5) REYNOLDS, A. J. 'A note on vortex-tube flows', *J. Fluid Mech.* 1962 **14** (No. 1), 18.

(6) SCHEPER, G. W. 'The vortex tube', *Refrigng Engng* 1951 **59** (October), 985, 1018.

(7) VAN DEEMTER, J. J. 'On the theory of the Ranque–Hilsch cooling effect', *Appl. scient. Res.* 1952 **3** (Section A, No. 3), 174.

(8) DEISSLER, R. G. and PERIMUTTER, M. 'An analysis of the energy separation in laminar and turbulent compressible vortex flow', 1958 (June), 40–53 (Heat Transfer and Fluid Mechanics Institute, University of California, Berkeley).

(9) DEISSLER, R. G. and PERIMUTTER, M. 'Analysis of flow and energy separation in a turbulent vortex', *Int. J. Heat Mass Transfer* 1960 **1**, 173.

(10) SUZUKI, M. 'Theoretical and experimental studies on the vortex tube', *Sci. Pap. Inst. phys. chem. Res., Tokyo* 1960 **54** (March), 43.

(11) BRUUN, H. H. Dissertation (in Danish), 1967, Fluid Mechanics Department, Technical University of Denmark.

(12) METENIN, V. I. 'Investigation of vortex temperature type compressed air separators', *Soviet Phys. Tech. Phys.* 1961 **5** (February), 1025.